Shock structure and spall behavior of porous aluminum

Cite as: AIP Conference Proceedings **2272**, 120015 (2020); https://doi.org/10.1063/12.0000913
Published Online: 04 November 2020

Zev Lovinger, Christophe Czarnota, Suraj Ravindran, Christian Kettenbeil, Alain Molinari, and G. Ravichandran

Shock Structure and Spall Behavior of Porous Aluminum

Zev Lovinger [1, a)], Christophe Czarnota[2, b)], Suraj Ravindran,[1, c)], Christian Kettenbeil[1, d)], Alain Molinari[2, e)] and G. Ravichandran[1, f)]

[1]*Division of Engineering and Applied Science, California Institute of Technology, Pasadena, CA, 91125, USA*
[2] *Université de Lorraine – CNRS – ENSAM, Laboratoire d'Etude des Microstructures et de Mécanique des Matériaux, LEM3, 57070 Metz, France*

[a)]*Corresponding author: lovinger@caltech.edu*

Abstract. Porous materials under shock and impact loading present significant potential for energy absorption and shock mitigation in various applications. Furthermore, additively manufactured materials which feature inherent levels of porosity due to the manufacturing process are increasingly used in shock applications. In this work, we have investigated porous 6061 aluminum samples with different levels of porosity, which were manufactured using a modified process of 3D printing. To achieve pores smaller than the 3D printing resolution (<50μm), the printing parameters were altered to control the pore sizes, resulting in porosities between 2%-10%. Plate impact experiments were conducted on these materials at pressures in the range of 2 to11 GPa, for which the free surface velocity was measured using a photonic Doppler velocimeter (PDV). The experiments were designed to extract both the shock structure properties and spall behavior. The structure of the steady shock was characterized as a function of porosity and shown to confirm trends revealed by the analytical approach (Czarnota et al, 2017), highlighting the importance of micro-inertia effects. The spall behavior was found to change significantly for the porous materials with respect to what was observed in dense materials. Mesoscale modeling has been carried out, to reveal the possible mechanisms underlying the observed phenomena.

INTRODUCTION

Shock compression of porous metals is of ongoing interest for its ability to mitigate impact and blast loadings [1-3]. Energy absorption is achieved mainly by large plastic deformations through pore collapse or crushing. These energy absorption and attenuation capabilities are of interest to defense technologies, for attenuating peak shocks and accelerations, protecting sensitive electronics or system components [4]. Furthermore, many materials contain some level of porosity, as an inherent outcome of its manufacturing process. As a consequence, and thus, much work has been done to characterize material response under shock loading, namely, measuring and developing equations of state (EOS), which account for the influence of the initial porosity [5-6]. In the past decade, interest in the behavior of porous metals under shock loading has increased, as additive manufacturing (AM) of metals is becoming a desirable manufacturing technology for shock applications. Current AM technologies introduce different levels of porosities, and their effects need to be explored, understood, and modeled properly to be accounted for correctly. Much work can be found in the literature to model the behavior of porous materials, accounting for pore collapse mechanisms, beginning with the fundamental works of Hermann [7] and later of Carrol and Holt [8]. Viscous and micro-inertia effects, the latter being related to the local acceleration fields around the collapsing pore, were identified as the main mechanisms, affecting the behavior of the porous media. In later years, different approaches have been examining the

Shock Compression of Condensed Matter - 2019
AIP Conf. Proc. 2272, 120015-1–120015-6; https://doi.org/10.1063/12.0000913
Published by AIP Publishing. 978-0-7354-4000-5/$30.00

dominance and importance of these two factors [9-11]. During the past two decades, Molinari and coworkers have developed several models, outlining the significance of micro-inertia to describe the shock structure of porous materials [12-14]. In recent work, Czarnota et al. [15] demonstrated a good comparison with experimental data, of the EOS of porous aluminum over a large range of porosities and shock levels. The comparison seems to capture also the non-linear behavior when combining lower porosities and low shock intensities [15]. Additionally, they have also implemented the effect of micro-inertia around pores, for the description of spall fracture in a high purity grade tantalum [13-14, 16]. Spall experiments of porous metals such as aluminum and copper were also studied in the literature [17-19] and yet, only limited work has been carried out to explain and capture the influence of porosity on the spall behavior of such materials.

In this work, an experimental campaign on porous aluminum alloy 6061 was carried out to examine both shock structure and spall behavior as a function of porosity and shock amplitude. The material with desired levels of porosity was manufactured using additive manufacturing (AM) technologies by altering the printing parameters to achieve the desired level of porosities and pore sizes. The experimental data was used to validate the effects of micro-inertia by comparison with predictions of the analytical model described in [15]. In addition, simplified mesoscale numerical modeling was used to examine the mechanisms responsible for the observed phenomena in the experiments.

EXPERIMENTAL: MATERIALS AND RESULTS

The plate impact experiments were conducted using the 38.7 mm bore (1.525-inch) powder-gun facility at Caltech. Figure 1(a) shows the experimental configuration of the plate impact experiments. The impactor was a 3mm steel plate, accelerated with a 76.2 mm (3-inch) long polycarbonate sabot, and the aluminum target had a thickness of 10-12 mm. The geometry was designed to achieve both a steady compressive shock and a spall response. The main diagnostics was a continuous measurement of the free surface velocity, using Photonic Doppler Velocimetry (PDV). Figures 1(b) and 1(c) show the assembly of the target on the alignment gimbal and the focused PDV probe on the back surface. The porous Al6061 samples were made using Additive Manufacturing (AM) technology. In order to achieve the desired parameters for the porosity, the AM parameters, namely the hatch spacing and the laser velocity have been modified after scanning a large range of combinations. The specifications for these samples were to achieve a homogeneous distribution of closed spherical pores, with an average diameter of 50μm or less, regular in shape. This designed AM process allowed reaching with these specifications, porosities in the range of 1%-8%. For the thicknesses of the samples and range of impact stresses, a steady shock was achieved for porosities up to 4%. Table 1 summarizes the experiments conducted in the present study. Four of the experiments were performed on fully dense samples – two of which were AM samples, and the other two were wrought Al6061 samples, which was used for comparison with a standard manufactured material.

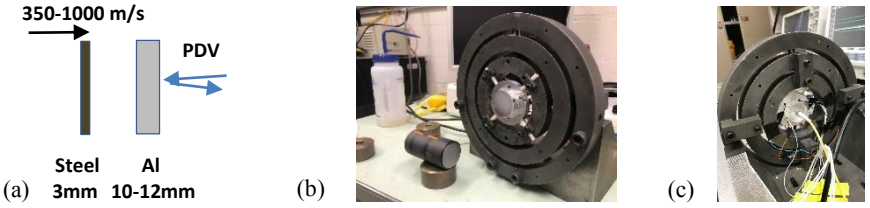

FIGURE 1. Plate impact experimental set up: (a) schematic, (b) target assembly on alignment gimbal and (c) PDV mounted on the back side.

Figure 2 shows the measured free surface velocity in each of the experiments. Fig. 2(a) shows a comparison between the wrought and fully dense AM samples at two shock levels (~5 and ~11 GPa). The measured shock structure and spall behavior for both AM and wrought fully dense materials are very similar. The differences in plastic wave speeds correspond to small differences in the material properties [20]. Figure 2(b) shows all the measured data for the porous samples for two ranges of porosities of ~2% and ~4% at three different shock levels. The analysis of the data addressed two aspects: (1) the plastic shock characteristics and their comparison with the prediction of the analytical model [15] and (2) the spall behavior. They are described in the following sections.

TABLE I. Experimental conditions of the plate impact experiments.

Experiment#	Porosity [%]	V_{Impact} [m/s]	Pressure, P [GPa]	Thickness, h [mm]
PA1802	0.0(W)*	467	5.0	11.87
PA1803	0.0	464	5.0	11.85
PA1804	0.0(W)*	985	11.6	11.89
PA1805	0.0	988	11.7	11.85
PA1806	4.0	992	9.5	11.90
PA1901	1.8	998	10.2	11.90
PA1902	2.7	552	4.7	11.89
PA1903	4.1	701	5.9	11.83
PA1905	2.0	365	2.5	11.78
PA1909	3.6	430	3.5	9.90

* (W) – denotes wrought fully dense material. All other materials are made using additive manufacturing (AM).

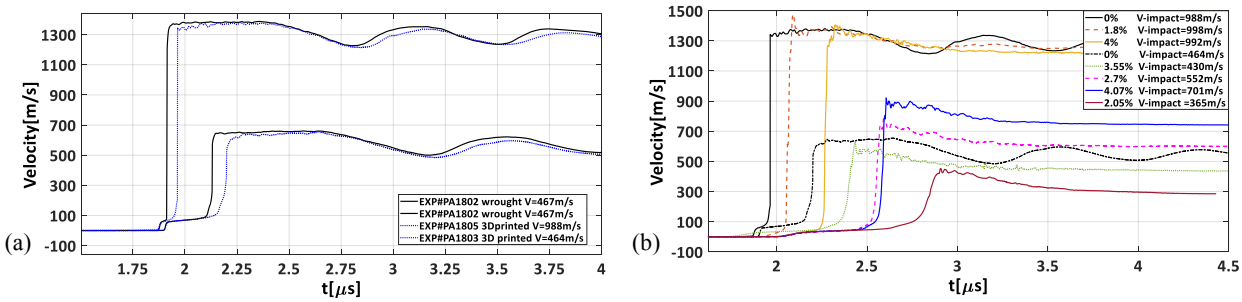

FIGURE 2. Measured free surface velocities: (a) comparison between wrought and AM (3D printed) material targets at two shock levels, (b) results for AM samples with different porosities and shock levels.

SHOCK WIDTH: COMPARISON WITH ANALYTICAL MODEL

The comparison of the results with the micro-inertia based analytical model was focused on the essential characteristics which could validate the presence of micro inertia effects as predicted by the model. Two model predictions were examined in light of the experimental data. The first relates to the change in shock width at different pressures. Czarnota et al. [15] have shown that the shock width does not change significantly for the same level of porosity when micro inertia is dominant and shows broadening in the low pressures range, where micro-inertia effects become small. For the two high shock amplitudes (around 5 and 11 GPa), the rise time remains nearly the same both for porosities of 2% and 4%, validating the prediction of the role of micro-inertia. Only for the very low pressures (around 2.5 GPa and 3.5 GPa), a significant shock broadening is observed, with a much longer rise time. This also matches very well with the prediction of the analytical model, which showed for these levels of porosities, a significant broadening of the shock width, for shock levels below ~4 GPa. At this lower pressure regime, micro-inertia effects become small, as demonstrated in Figure 13 in [15]. The second aspect for comparison is the relation between shock-velocity and particle-velocity(U_s-u_p), referring to the material's EOS. Figure 3 shows the plots of shock velocity vs. particle velocity (U_s-u_p) predicted relations of the analytical model in [15], with iso-shock level contours shown as dotted lines. A key step for the formulation in [15] is the analytical characterization of the quasi-static compression curve, which for weak shocks (up to 8GPa for porous aluminum) were used in place of the Hugoniot for shock analysis. The data deduced from the current experiments are plotted as closed shaded circles. The comparison was found to be good for all the experimentally measured points, including those in the non-linear regime at lower pressures. A small discrepancy of 1.5-2%, could be seen for the fully dense AM manufactured specimens with respect to the fully dense Al6061 linear U_s-u_p relation. As mentioned previously, this could be explained by small differences in the elastic properties and densities of the fully dense wrought and AM Al6061materials [20].

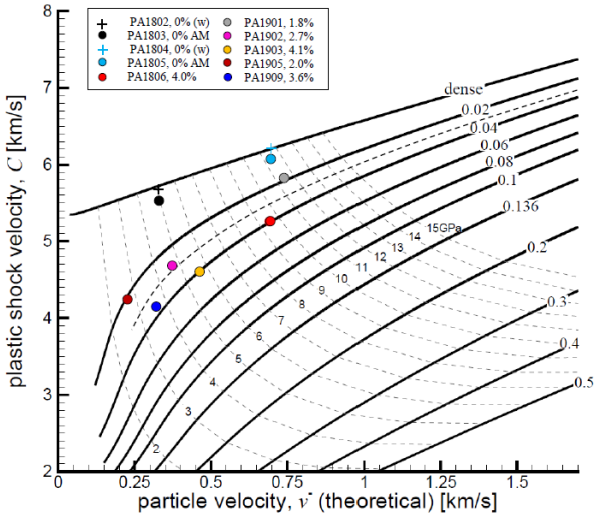

FIGURE 3. Shock velocity vs. particle velocity (*Us-Up*) space obtained from the analytical model [15] and the data points of currently measured data in solid filled circles. The light dotted lines plotted are iso-shock levels.

SPALL BEHAVIOR IN POROUS MATERIALS

The calculated spall strength was very similar for both the fully dense Al6061 AM and wrought materials and compares very well with the standard spall strength for this material of ~1.2 GPa [21]. The differences in spall behavior of the porous samples in comparison with the full dense ones are evident from the results reported in Fig. 2. In comparison with the ringing pullback signal associated with dense materials, after reaching a maximum level, the velocity is reduced to a lower value and no spall signal emerges. Two additional observations can be made: (1) the decreased velocity level is close to that of the minimum value of the fully dense pull-back signal but slightly larger. This is a puzzling result as to why the corresponding spall strength would *increase* for the porous material; (2) the magnitude of the pull-back velocity remains almost the same for the range of porosities and pressures examined here. In order to understand the underlying reasons for these observations, a mesoscale numerical model was used. The model (LS-DYNA, [22]) is a simplified 2D strip of the shock specimen geometry. The porous material is built as an idealized representation, using a unit cell with the average pore diameter of 50μm in diameter and the cell size is set to reach the desired porosity. The 2D strip included two arrays of unit cells for the actual thicknesses of the flyer and target, as shown in Fig. 4.

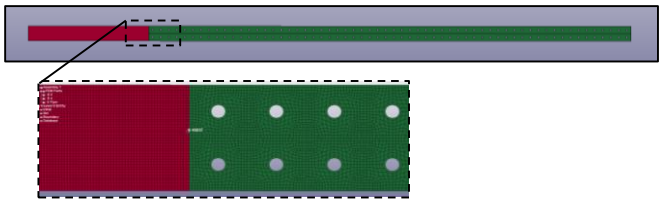

FIGURE 4. A mesoscale numerical model of the impact experiment on a porous sample. The unit cell geometry represents the actual porosity of the AM material in the experiments.

Figure 5 shows the results obtained from the numerical modeling, considering an initial porosity of 4%. The numerical model captures the observed relaxation in the free surface velocity profile, as shown in Fig. 5(a) obtained for two values of spall strength, 1.2GPa which matches well with the pull-back signal of the fully dense samples, and a larger value of 2 GPa. The larger spall strength was adopted to match the relaxation of the pull-back signal seen in

the experiment. For the large spall strength, the model initially shows a stronger pull back at ~2.9 μs, before relaxing to the final value of the free surface velocity. This could be due to the idealization of the model with a single pore size in contrast to the actual material that includes a span of sizes and shapes, which could result at a smoother decay of the pull-back signal. A peculiar behavior observed in the numerical simulations was an opening mode of the collapsed pores, which could be a possible "structural" response at the mesoscale level, see Fig 5(b). This behavior will be affected by the material response during the pore collapse. Figure 5(c) shows the plastic strain distribution around the pores, after their closure. A large area around the pores undergoes large plastic strains of 0.2 to 0.8, which could result in a significant hardening of the pre-shocked porous material prior to spall. These preliminary results need to be further explored to investigate these complex phenomena of pore collapse during shock compression and expansion during spall.

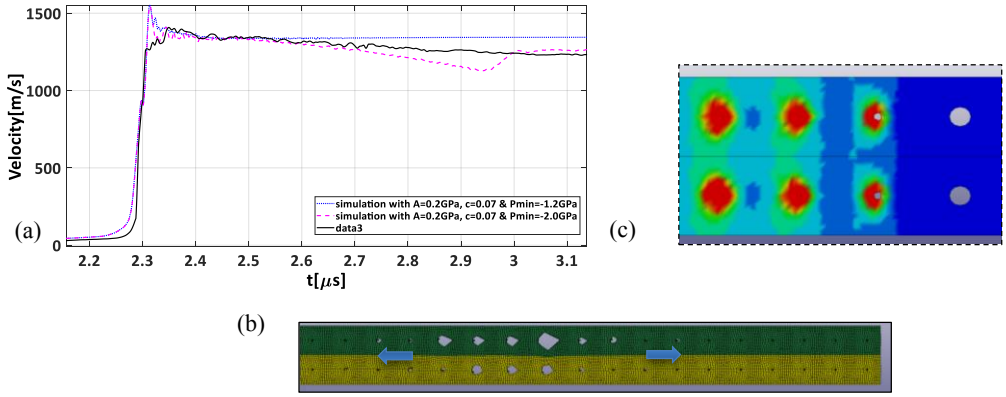

FIGURE 5. Results of the mesoscale numerical model: (a) comparison of the pull-back velocity signal from the experiment PA1806 for two values of spall strength, (b) geometry of the pores at 3.1 μs after impact showing reopening of the pores, (c) plastic strains around the closing pores (maximum saturated value in the middle is plastic strain of 0.5).

SUMMARY AND CONCLUSIONS

A series of shock experiments was conducted on 6061 aluminum samples with porosities of 0-4% to examine shock structure and spall behavior, at shock levels of 2-11 GPa. The materials were manufactured using AM technology with modified parameters to achieve an average pore diameter of 50 μm. The experiments confirm the important role of micro-inertia effects on the steady shock structure, illustrated by the theoretical model of Czarnota et al. [15]. The analytical model results match many of the experimentally measured behaviors, underlining the importance of micro-inertia and its essential role in structuring the shock front. The spall behavior of porous aluminum introduces complex phenomena of "pulling" on closed pores, demonstrating a possible structural response, at the mesoscale level, due to reopening of the pores. A numerical model was used to examine these mechanisms, suggesting the post-shocked material, due to the significant plastic strains around the shock collapsed pores, could result in a hardened spall response.

ACKNOWLEDGMENTS

The authors would like to acknowledge the work of Jacob Nuechterlein and Adam J. Polizzi from Elementum 3D for the design and manufacturing of the AM materials used in this work. The authors would like to thank Dr. Branden Kappes and Professor Aaron Stebner from the Colorado School of Mines for conducting micro-tomography on the porous samples.

REFERENCES

1. V. F. Nesterenko, *Dynamics of heterogeneous materials*, Springer-Verlag, New York (2001)
2. P. D. Smith and J. G. Hetherington, *Blast and Ballistic Loading of structures*, Butterworth-Heinemann Ltd., Oxford, (1994).
3. M. D. Goel, Ph. Altenhofen, V. A. Matsagar, A. K. Gupta, Ch. Mundt, and S. Marburg, Comb. Expl. And Shock waves, **15**, 373-380 (2015).
4. L. Bin Chao, Z. Gui Ping and L. Tian Jian, Science China **55**, 451-463, (2012).
5. A. B. Medvedev and R. F. Trunin, Physics-Uspekhi **55**, 773–789 (2012).
6. R. G. McQueen, S. P. Marsh, J. W. Taylor, J. N. Fritz, and W. J. Carter in *High-Velocity Impact Phenomena*, edited by R. Kinslow, Academic Press, New York, Chap VII, (1970).
7. W. Hermann, J. Appl. Phys. **40**, 2490-2499 (1969).
8. M. M. Carroll and A. C. Holt, J. Appl. Phys. **43**, 1626-1636, (1974).
9. J. N. Johnson, J. Appl. Phys. **52**, 2812-2825 (1981).
10. M. Ortiz and A. Molinari, J. Appl. Mech. **114**, 48-53 (1992).
11. T. Cohen and D. Durban, Int. J. Solids. Struct. **71**, 70-78 (2015).
12. A. Molinari and S. Mercier, J. Mech. Phys. Solids, **49**, 1497-1516 (2001).
13. C. Czarnota, N. Jacques, S. Mercier and A. Molinari, J. Mech. Phys. Solids, **56**, 1624-1650 (2008).
14. N. Jacques, C. Czarnota, S. Mercier and A. Molinari, Int. J. Fract. **162**, 159-175 (2010).
15. C. Czarnota, A. Molinari and S. Mercier, J. Mech. Phys. Solids, **107**, 204-228 (2017).
16. C. Czarnota, S. Mercier and A. Molinari, Int. J. Fract. **141**, 177-194 (2006).
17. R. G. Kraus, D. J. Chapman, W. G. Proud and D. C. Swift, J. Appl. Phys. 105, 114914 (2009).
18. S. Bonnan, P. L. Hereil, and F. Collombet, J. Appl. Phys. **83**, 5741 (1998).
19. R. R. Boade, J. Appl. Phys, **39**. 5693 (1968).
20. Datasheet for RAM Al6061 at www.elementrum3d.com.
21. D. J. Steinberg, Technical Report: UCRL-MA-106439, (1996).
22. Livermore Software Technology Corporation, *LS-DYNA keyword user's manual*, R.9.01, (2016).